PROCEEDINGS, 50th Workshop on Geothermal Reservoir Engineering
Stanford University, Stanford, California, February 10-12, 2025
SGP-TR-229

Elucidating the Alkali-Activated Dissolution Mechanisms in Boehmite-Based Cementitious Composites Under Enhanced Geothermal Conditions Using In-situ Synchrotron Characterization

Sizhan Liu[1], Michelle Devoe[1], Toshifumi Sugama[1], Jianming Bai[2], Tatiana Pyatina[1]

1) Interdisciplinary Science Department, Brookhaven National Lab, Upton NY 11973

2) National Synchrotron Light Source II, Brookhaven National Lab, Upton NY 11973

tpyatina@bnl.gov, jmbai@bnl.gov

Keywords: enhanced geothermal systems, in-situ synchrotron X-ray diffraction, alkali activation, aluminum oxyhydroxide, quantitative analysis, Rietveld refinement.

ABSTRACT

The widespread adoption of enhanced geothermal systems has the potential to revolutionize global renewable electrical power access. However, its progress is currently obstructed by the inability of traditional cement formulations to endure high-temperature corrosive conditions. This study focuses on a novel alkali-activated boehmite cementitious system specially designed for enhanced geothermal wells, where rationalizing the thermal-induced phase transitions is pivotal for their mechanical performance under high-temperature and high-pressure environments. During the hardening process of alkali-activated cements, a complex interplay of dissolution and crystallization processes takes place, critically influencing the development of mechanical properties. Utilizing synchrotron-based hard X-ray diffraction, we investigate these dynamics in real-time to elucidate the mechanisms underpinning the solidification process under EGS relavent conditions. The solidification mechanism established in this work provides valuable insights for optimizing the performance of alkali-activated boehmite cementitious materials for high-temperature geothermal applications.

1. INTRODUCTION

The transition to renewable energy sources is crucial for addressing global energy demands and mitigating climate change. Among these, geothermal energy stands out for its potential to provide a reliable and sustainable supply of baseload power. Enhanced Geothermal Systems (EGS) represent a promising avenue for expanding geothermal energy adoption (Jolie et al., 2021; Mitigation, 2011). Unlike wind or solar energy, geothermal power provides consistent electricity generation independent of weather or seasonal variations, making it a critical component for grid stability. However, the large-scale realization of EGS faces significant technical challenges, particularly in the construction and longevity of geothermal wells. These wells must operate under extreme subsurface conditions, including temperatures exceeding 300°C, high pressures, and chemically aggressive fluids (Fridleifsson and Elders, 2005). Such conditions pose severe challenges for conventional cementitious materials, which often suffer from degradation, cracking, or loss of structural integrity (Sircar et al., 2022). Failures in well cement systems can lead to fluid leakage, reduced efficiency, and costly maintenance, threatening the feasibility of EGS projects. Addressing these issues requires the development of advanced cementitious materials that not only withstand these extreme environments but also maintain long-term stability and performance.

The solidification process of cementitious materials under EGS conditions is highly sensitive to temperature, which plays a decisive role in phase selection and reaction dynamics (Pyatina and Sugama, 2020; Pyatina et al., 2024). Alkali addition further influences these processes by modulating the dissolution rates of ions and the mass exchange processes in response to temperatures (Aldabsheh et al., 2015; Deng et al., 2020; Zhu et al., 2024). This dual control of thermodynamic and kinetic factors makes the solidification of cement at high temperatures a complex process involving both equilibrium and non-equilibrium phenomena. By regulating these interactions, the alkali environment governs transformation pathways and ultimately determines the material's performance under extreme conditions.

In alkali-activated materials, pH regulation plays a pivotal role in controlling reaction rates and determining final binding phases, which are critical for achieving durable and thermally stable materials (Kryvenko et al., 2024; Mendes et al., 2021). Unlike traditional alkali-activated systems that rely on the dissolution of aluminosilicate precursors in alkaline solutions followed by polycondensation into a solid, gel-like network (Nodehi and Taghvaee, 2022), we select aluminum hydroxide ($Al(OH)_3$) as a precursor. The absence of silicon shifts the primary role of alkali to facilitating the dehydroxylation of $Al(OH)_3$ under hydrothermal conditions, leading to the formation of aluminum oxyhydroxide (boehmite, γ-AlOOH). Previous studies have shown that the transformation of $Al(OH)_3$ to γ-AlOOH involves two reaction mechanisms: a solid-state mechanism and a dissolution-precipitation mechanism (Gong et al., 2003; Lopushan et al., 2007; Zhang et al., 2019). The primary distinction between these two lies in whether aqueous Al ions participate in the formation of boehmite. Therefore, investigating the dissolution of Al ions is crucial for understanding the formation mechanism of the boehmite phase. Here, we utilize in-situ synchrotron X-ray diffraction to investigate the dissolution behavior of aluminum species during the solidification of boehmite-based cementitious materials (BBCMs) under hydrothermal alkali influence at EGS relevant temperature. This technique enables real-time monitoring of dynamic phase transformations, providing critical insights into the mechanisms driving the development of high-performance cement for extreme geothermal environments.

2. QUANTITATIVE ANALYSIS USING SYCHRONTRON X-RAY DIFFRACTION

X-ray diffraction (XRD) is a widely used technique for characterizing the crystalline structure of materials. In particular, high-energy in-situ synchrotron XRD technique leverages the stable, high-flux beam provided by a synchrotron source to ensure consistent beam penetration with a defined sample volume, enabling real-time monitoring of phase evolution. This technique offers critical insights into dynamic structural evolutions, including phase transitions, crystallization, dissolution, and decomposition. It also supports experiments under various controlled environments, such as hydrothermal conditions, elevated temperatures, magnetic fields, and other external stimuli. Quantitative analysis of crystalline phases is achieved through Rietveld refinement using Topas-academic (Coelho, 2018). In Rietveld refinement, the relative contributions of different crystalline phases are determined by refining structural parameters and scale factors obtained from diffraction data. A fundamental equation for calculating the weight fraction of a given crystalline phase is expressed as follows (Dinnebier and Billinge, 2015; Le Saoût et al., 2011; Snyder and Bish, 1989):

$$w_1 = \frac{s_1 m_1 V_1}{\sum_{i=1}^{p} s_i m_i V_i}$$

, where w_1 is the weight fraction of phase 1, s_1, m_1, and V_1 are the scale factor, relative atomic mass, and unit cell volume of phase 1, respectively, and p represents the total number of crystalline phases in the system. The stable high flux of the synchrotron X-ray source ensures scale factors proportional to the effective scattering volume of certain materials.

The content of element X in phase 1 can be determined using:

$$\frac{\sum_{i=1}^{p} s_i m_i V_i \times w_1}{m_1} n_1 = s_1 V_1 n_1$$

, where n_1 is the number of X atoms in the formula of phase 1 with relative atomic mass m_1. The total content of element X in all crystalline phases of the system at a given temperature t_0 can be expressed as:

$$\mathrm{mol}(\mathrm{X}, t_0) = \sum_{i=1}^{p} s_i V_i n_i$$

If amorphous phases are present, their molar percentage at temperature t can be calculated using:

$$\mathrm{mol\%}(\mathrm{Amorphous}, t) = 1 - \frac{\mathrm{mol}(\mathrm{X}, t)}{\mathrm{mol}(\mathrm{X}, t_0)}$$

, where t_0 serves as the baseline reference point for the calculation, typically chosen when the material has the highest X in the crystalline phase to ensure that the calculated amorphous phase molar fraction is greater than zero.

3. HYDROTHERMAL IN-SITU CELL DESIGN

To conduct in-situ synchrotron experiments under hydrothermal conditions, a specially designed reaction cell is required to withstand harsh alkaline environments and high-temperature conditions. For alkali-activated materials, the highly alkaline environment necessitates excellent corrosion resistance in the reaction vessel. Teflon, being chemically inert and resistant to strong alkalis, was chosen as the reaction container. Its high melting point (>300°C) ensures compatibility with hydrothermal conditions below this temperature. To enhance mechanical strength and prevent deformation during prolonged heating, the Teflon capillary was inserted into a quartz tube, which provides high thermal stability and resistance to mechanical stress. The single diffraction peak of Teflon at low angles, which shifts continuously with temperature, minimizes interference with sample analysis. After loading the sample into the Teflon capillary, both ends were sealed using steel rods and high-temperature sealant to ensure tight sealing and pressure stability. The quartz tube housing the Teflon capillary was also sealed at both ends with appropriate sealant to maintain integrity. The X-ray beam was aligned with the sample at the center of the Teflon capillary, ensuring optimal signal collection, while the coil heater wrapped around the quartz tube provided uniform heating, as shown in Figure 1.

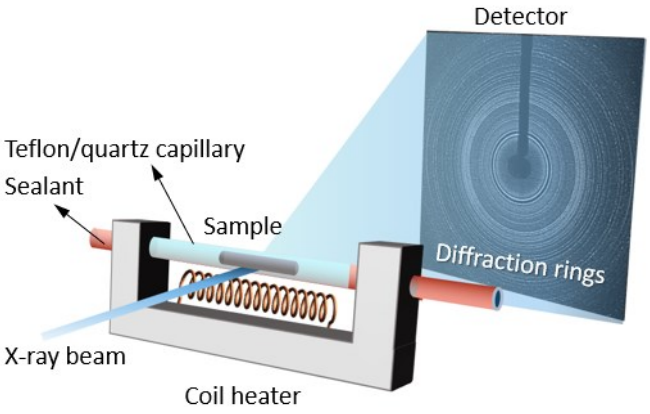

Figure 1: Schematic representation of the hydrothermal in-situ cell design used for synchrotron X-ray diffraction experiments. The reaction cell consists of a Teflon capillary enclosed within a quartz tube for enhanced mechanical strength and thermal stability. The Teflon capillary, sealed at both ends with steel rods and sealant, houses the sample. The quartz tube, also sealed with appropriate sealant to ensures cell integrity under high temperature. The X-ray beam passes through the sample, and the resulting diffraction patterns are collected by the detector. A coil heater provides uniform heating across the sample to maintain stable hydrothermal conditions.

4. IN-SITU CHARACTERIZATION OF SOLIDIFICATION OF BBCM

In this study, we performed a quantitative analysis to investigate the hydrothermal transformation of aluminum hydroxide precursors into aluminum oxyhydroxide using time-resolved in-situ synchrotron XRD at 28-ID-1 (PDF) beamline at Brookhaven National Laboratory. The wavelength of the X-ray beam was 0.1665 Å, and the spot size at the sample was 0.5 mm (horizontal) × 0.5 mm (vertical).The samples consisted of aluminum hydroxide and Na_2SiO_3 (sodium metasilicate, SMS) with mass percentages of 0%, 3%, and 9%, prepared at a water-to-solid mass ratio of 1:2. This study explored how adding SMS as an alkaline activator adjusts the solubility of aluminum ions at varying temperatures, which in turn controls the transformation rate to aluminum oxyhydroxide, a critical step in the solidification process of BBCMs. Figure 2 illustrates the observed crystalline phase transformation at 250°C from aluminum hydroxide to aluminum oxyhydroxide under alkaline concentrations of 0%, 3%, and 9% derived from Rietveld refinement of the in-situ XRD data. The trend in the results suggests that the alkaline concentration is a key factor in governing the dynamics of boehmite formation. However, what are the dynamics of the non-crystalline phase formation during this process—such as the dissolution of aluminum and the formation of amorphous phases?

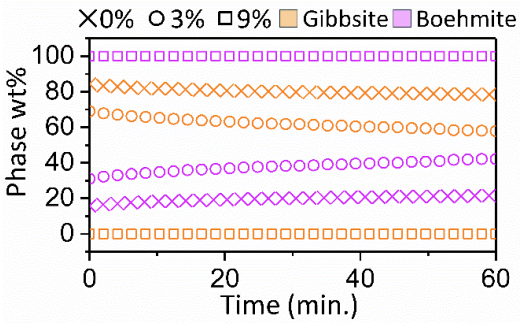

Figure 2: Phase evolution from gibbsite to boehmite at 250°C over 60 minutes under different alkaline concentrations of 0%, 3%, and 9%.

To address this question, we conducted a quantitative analysis to evaluate the evolution of the non-crystalline phase. The stable flux of the synchrotron X-ray source and sufficiently large beam size ensure a scattering volume that is statistically representative of the overall chemical reaction, enabling the total elemental content within the scattering volume to remain largely constant throughout the experiment. Taking advantage of these features, the aluminum content in the crystalline phase at the onset of the isothermal hold at 250°C was defined as the baseline for quantifying its evolution over time. The calculated amorphous phase reflects an increase relative to the baseline, though other amorphous phases may already exist in the baseline, which are not discussed here.

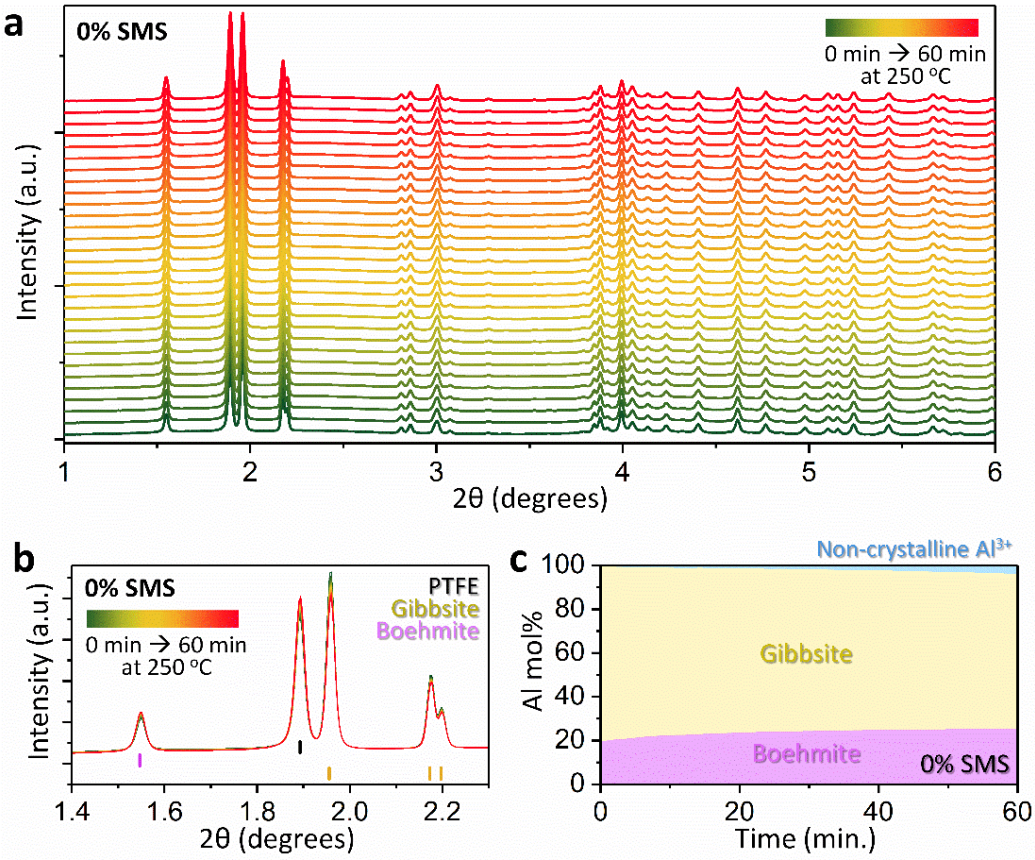

Figure 3: In-situ synchrotron XRD analysis of the hydrothermal transformation at 250°C under 0% SMS conditions. (a) Time-resolved XRD patterns showing the evolution of crystalline phases (gibbsite and boehmite) over 60 minutes. The color gradient represents the time progression from 0 minutes (green) to 60 minutes (red). (b) Zoomed-in view of the low-angle XRD peaks corresponding to PTFE, gibbsite, and boehmite. (c) Quantitative phase analysis based on Rietveld refinement, illustrating the molar percentage of aluminum in gibbsite, boehmite, and the non-crystalline phase.

As shown in Figure 3a, we first examined the structural evolution at 250°C using in-situ synchrotron XRD under SMS-free conditions. The zoomed-in view in Figure 3b highlights changes in low-angle XRD peaks corresponding to PTFE, gibbsite, and boehmite. The data indicates that at 250°C, the peak intensities of gibbsite and boehmite exhibit minimal variation, indicating the slow kinetics of boehmite formation, characterized by negligible peak intensity change over time. Quantitative refinement results, as presented in Figure 3c, further confirm this slow transformation rate. Only a small amount of non-crystalline phase formation was observed during the experiment, suggesting that aluminum dissolution is significantly restricted in the absence of alkaline activators.

When the SMS content is increased to 3%, the XRD patterns of the gibbsite-to-boehmite transformation under hydrothermal conditions at 250°C within a one-hour timeframe are illustrated in Figure 4a. Figure 4b shows the low-angle XRD peaks, where a decrease in the intensity of the gibbsite peak at ~1.95° is observed, indicating a reduction in the crystalline gibbsite phase. In contrast, the boehmite peak at ~1.55° exhibits minimal changes in intensity, suggesting that gibbsite dissolution occurs, but the formation of crystalline boehmite remains limited. This observation is further supported by the evolution of the Al distribution shown in Figure 4c. The molar fraction of Al in the gibbsite phase decreases over time, accompanied by an increase in the non-crystalline Al fraction, whereas the change in the boehmite phase is comparatively minor. These trends suggest that, under 3% SMS conditions, the rate of gibbsite decomposition/dissolution exceeds the rate of crystalline boehmite formation. The continuous increase in the non-crystalline Al fraction, without reaching a plateau within the experimental timeframe, indicates that gibbsite dissolution/decomposition is governed by slow kinetics at 250°C. While the addition of SMS appears to accelerate this process, equilibrium is not achieved within the one-hour timeframe. Additionally, further investigation is needed to confirm whether the Al released from gibbsite contributes to the formation of amorphous solid phases or exists as dissolved aqueous Al species within the non-crystalline phases.

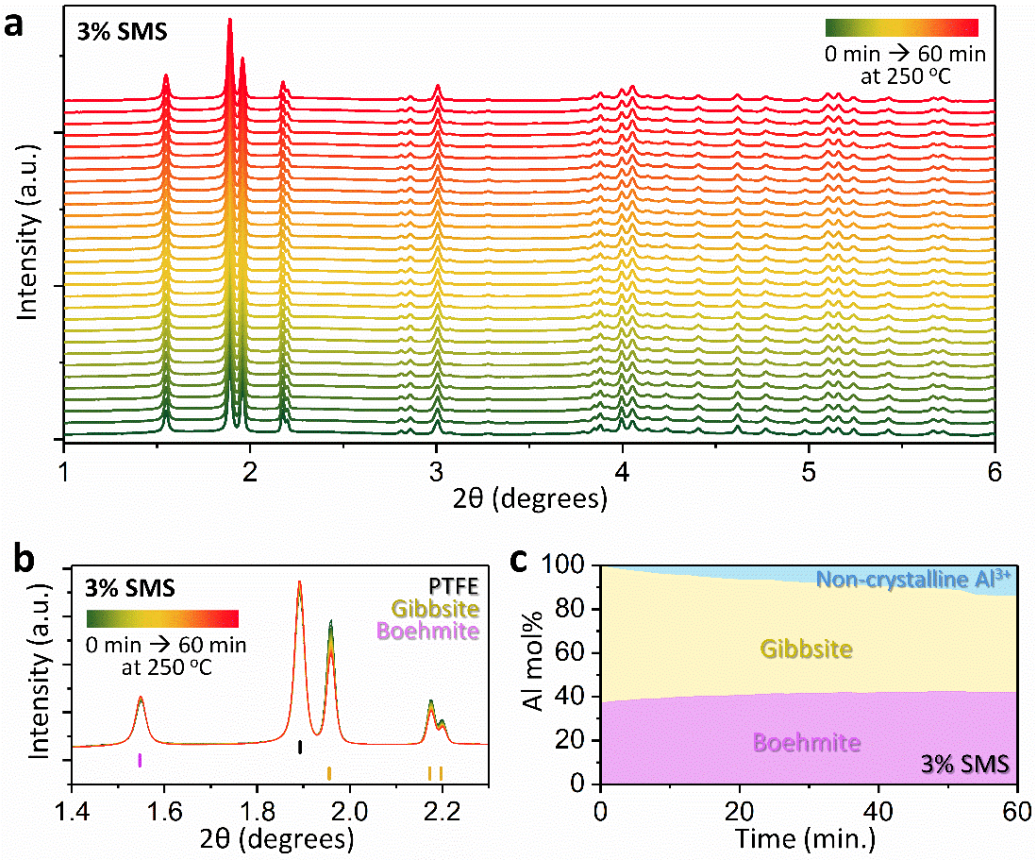

Figure 4: In-situ synchrotron XRD analysis of the hydrothermal transformation at 250°C under 3% SMS conditions. (a) Time-resolved XRD patterns showing the evolution of crystalline phases (gibbsite and boehmite) over 60 minutes. The color gradient represents the time progression from 0 minutes (green) to 60 minutes (red). (b) Zoomed-in view of the low-angle XRD peaks corresponding to PTFE, gibbsite, and boehmite. (c) Quantitative phase analysis based on Rietveld refinement, illustrating the molar percentage of aluminum in gibbsite, boehmite, and the non-crystalline phase.

When the SMS content is increased to 9%, the XRD patterns during the isothermal hold at 250°C for one hour are presented in Figure 5a. In comparison to Figures 3a and 4a, these patterns exhibit notable differences. For the 0% and 3% SMS samples, the initial time point was used as the reference for the non-crystalline phase calculation due to the higher Al content observed in the crystalline phases. However, for the 9% SMS sample, the 60-minute time point was selected as the reference, as it exhibited the highest Al content in the crystalline phases during the experiment. As shown in Figure 5b, the boehmite peak is broader compared to the 0% and 3% SMS samples, while the gibbsite peak is no longer present, indicating its complete dissolution/decomposition. The broader boehmite peak suggests a smaller crystallite size in the 9% SMS sample. Additionally, $NaAlO_2$ emerges as a new crystalline phase under these conditions. The boehmite phase shows minimal intensity changes over time, while the non-crystalline Al appears to transform into the $NaAlO_2$ phase, as illustrated in Figure 5c. These results suggest that, in the absence of gibbsite, the non-crystalline Al does not convert into boehmite. Instead, under high Na concentrations, it preferentially forms NaAlO2, exhibiting the distinct role of alkali in governing the phase transformation pathways.

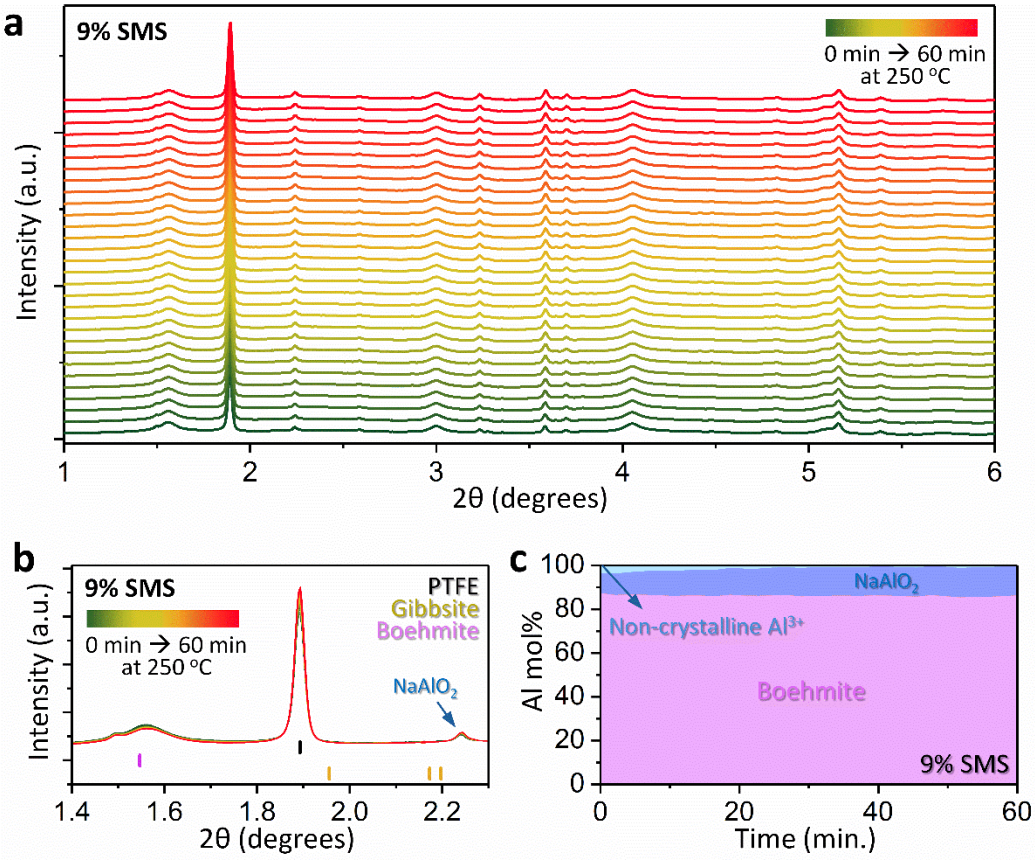

Figure 5: In-situ synchrotron XRD analysis of the hydrothermal transformation at 250°C under 9% SMS conditions. (a) Time-resolved XRD patterns showing the evolution of crystalline phases (gibbsite and boehmite) over 60 minutes. The color gradient represents the time progression from 0 minutes (green) to 60 minutes (red). (b) Zoomed-in view of the low-angle XRD peaks corresponding to PTFE, gibbsite, and boehmite. (c) Quantitative phase analysis based on Rietveld refinement, illustrating the molar percentage of aluminum in gibbsite, boehmite, and the non-crystalline phase.

5. CONCLUSION

From a practical EGS perspective, the solidification process of BBCMs must account for the variations in temperature associated with increasing geological depth. These temperature differences significantly influence the role of the alkali activator during the solidification process. In this study, we selected 250°C as a representative temperature to investigate the effects of varying alkali concentrations on the reaction pathways. Our findings reveal distinct reaction mechanisms under different alkali conditions, with the presence of non-crystalline phases—including aqueous Al ions dissolved from gibbsite and newly formed amorphous phases—playing a pivotal role in boehmite formation. These non-crystalline phases act as intermediates, influencing the crystallization kinetics and the development of the final microstructure, which directly impacts the material's mechanical performance. Further studies linking mechanical properties, phase evolution, and microstructural development are essential to fully evaluate the reliability of BBCMs under EGS conditions. The synchrotron-based experimental approach and analytical framework demonstrated in this study can also be extended to other alkali-activated systems, enabling precise control over the structure-mechanical performance relationship for EGS wells operating under extreme conditions.

ACKNOWLEDGEMENT

This work was supported by the U.S. Department of Energy, Office of Science supporting the Energy Earth-shotTM Initiative, as part of the “Center for Coupled Chemo-Mechanics of Cementitious Composites for EGS (C4M)” project at Brookhaven National Laboratory under contract number 2026-BNL-IS012-FUND. This research used 28-ID-1 (PDF) and 28-ID-2 (XPD) beamlines at the National Synchrotron Light Source II, a U.S. DOE Office of Science User Facility operated for the DOE Office of Science by Brookhaven National Laboratory under contract no. DE-SC0012704.

REFERENCES

Aldabsheh, I., Khoury, H., Wastiels, J., Rahier, H., 2015. Dissolution behavior of Jordanian clay-rich materials in alkaline solutions for alkali activation purpose. Part I. Applied Clay Science 115, 238-247.

Coelho, A.A., 2018. TOPAS and TOPAS-Academic: an optimization program integrating computer algebra and crystallographic objects written in C++. Journal of Applied Crystallography 51(1), 210-218.

Deng, G., He, Y., Lu, L., Hu, S., 2020. The effect of activators on the dissolution characteristics and occurrence state of aluminum of alkali-activated metakaolin. Construction and Building Materials 235, 117451.

Dinnebier, R.E., Billinge, S.J., 2015. Powder diffraction: theory and practice. Royal society of chemistry.

Fridleifsson, G.O., Elders, W.A., 2005. The Iceland Deep Drilling Project: a search for deep unconventional geothermal resources. Geothermics 34(3), 269-285.

Gong, X., Nie, Z., Qian, M., Liu, J., Pederson, L.A., Hobbs, D.T., McDuffie, N.G., 2003. Gibbsite to Boehmite Transformation in Strongly Caustic and Nitrate Environments. Industrial & Engineering Chemistry Research 42(10), 2163-2170.

Jolie, E., Scott, S., Faulds, J., Chambefort, I., Axelsson, G., Gutiérrez-Negrín, L.C., Regenspurg, S., Ziegler, M., Ayling, B., Richter, A., 2021. Geological controls on geothermal resources for power generation. Nature Reviews Earth & Environment 2(5), 324-339.

Kryvenko, P., Rudenko, I., Sikora, P., Sanytsky, M., Konstantynovskyi, O., Kropyvnytska, T., 2024. Alkali-activated cements as sustainable materials for repairing building construction: a review. Journal of Building Engineering, 109399.

Le Saoût, G., Kocaba, V., Scrivener, K., 2011. Application of the Rietveld method to the analysis of anhydrous cement. Cement and concrete research 41(2), 133-148.

Lopushan, V.I., Kuznetsov, G.F., Pletnev, R.N., Kleshev, D.G., 2007. Kinetics of phase transitions of gibbsite during heat treatment in air and in water vapor. Refractories and Industrial Ceramics 48(5), 378-382.

Mendes, B.C., Pedroti, L.G., Vieira, C.M.F., Marvila, M., Azevedo, A.R., De Carvalho, J.M.F., Ribeiro, J.C.L., 2021. Application of eco-friendly alternative activators in alkali-activated materials: A review. Journal of Building Engineering 35, 102010.

Mitigation, C.C., 2011. IPCC special report on renewable energy sources and climate change mitigation. Renewable Energy 20(11).

Nodehi, M., Taghvaee, V.M., 2022. Alkali-activated materials and geopolymer: a review of common precursors and activators addressing circular economy. Circular Economy and Sustainability 2(1), 165-196.

Pyatina, T., Sugama, T., 2020. Cements with supplementary cementitious materials for high-temperature geothermal wells. Geothermics 86, 101840.

Pyatina, T., Sugama, T., Moghadam, A., Naumann, M., Skorpa, R., Feneuil, B., Soustelle, V., Godøy, R., 2024. Assessment of Cementitious Composites for High-Temperature Geothermal Wells. Materials 17(6), 1320.

Sircar, A., Solanki, K., Bist, N., Yadav, K., 2022. Enhanced Geothermal Systems–promises and challenges. International Journal of Renewable Energy Development 11(2), 333-346.

Snyder, R., Bish, D.L., 1989. Quantitative analysis. Modern powder diffraction 20, 101-144.

Zhang, X., Cui, W., Hu, J.Z., Wang, H.-W., Prange, M.P., Wan, C., Jaegers, N.R., Zong, M., Zhang, H., Pearce, C.I., Li, P., Wang, Z., Clark, S.B., Rosso, K.M., 2019. Transformation of Gibbsite to Boehmite in Caustic Aqueous Solution at Hydrothermal Conditions. Crystal Growth & Design 19(10), 5557-5567.

Zhu, X., Luan, M., Tang, D., Yang, K., Yang, C., 2024. Understanding the setting behaviours of alkali-activated slag from the dissolution-precipitation point of view. Cement and Concrete Composites 148, 105474.